JOURNAL OF GEOPHYSICAL RESEARCH, VOL. 105, NO. B6, PAGES 13,643–13,653, JUNE 10, 2000

Dynamics of dip-slip faulting: Explorations in two dimensions

David D. Oglesby[1] and Ralph J. Archuleta

Department of Geological Sciences and Institute for Crustal Studies, University of California, Santa Barbara

Stefan B. Nielsen[2]

Institute for Crustal Studies and Materials Research Laboratory, University of California, Santa Barbara

Abstract. Dynamic models of earthquake rupture and slip are a powerful method by which to investigate the physics of earthquakes. Owing to both conceptual and computational constraints, dynamic earthquake models have largely been limited to cases with geometrical symmetry, such as faults in unbounded media or vertical faults. However, there are both observational and theoretical reasons to believe that nonvertical dip-slip faults behave differently from faults with more symmetrical geometries. Previous observations have shown greater ground motion from thrust/reverse faults than normal faults and higher ground motion on hanging walls than on footwalls. In the present work, two-dimensional dynamic simulations of thrust/reverse and normal earthquakes show precisely these effects and also elucidate their causes. For typical nonvertical dip-slip faults the breakdown of symmetry with respect to the free surface allows radiated seismic waves to reflect off the free surface and to hit the fault again, altering the stress field on the fault. This process can lead to time-dependent normal stress and a feedback between the friction/rupture processes and seismic radiation. This interaction leads to thrust/reverse faults producing much higher fault and ground motion than normal faults with the same geometry and stress magnitudes. The asymmetric geometry also directly leads to higher motion on the hanging walls of such faults than on the footwalls. Simulations show that these effects occur for a variety of dip angles but only for faults that either intersect or closely approach the free surface. The results emphasize the strong effect that the free surface can have on the dynamics of fault rupture and slip.

1. Introduction

One of the primary goals of earthquake seismology is to understand the cause of strong ground motion at the Earth's surface. The case of dip-slip (thrust/reverse and normal) faulting warrants special attention because in many areas the largest seismic hazard lies in such faults. For example, in the western United States the 1971 San Fernando earthquake [*Trifunac and Hudson*, 1971], the 1992 Petrolia earthquake [*Shakal et al.*, 1992], and the 1994 Northridge earthquake [*Shakal et al.*, 1994] were all thrust earthquakes that occurred in the compressive tectonic regimes of northern and southern coastal California. Likewise, the 1954 $M = 6.0$ Rainbow Mountain–Fairview Peak–Dixie Valley sequence [*Romney*, 1957], the 1959 $M = 7.3$ Hebgen Lake earthquake [*U.S. Coast and Geodetic Survey*, 1959], and the 1983 $M = 6.9$ Borah Peak earthquake [*Reagor and Baldwin*, 1984] occurred in the tensional environment of the Basin and Range. Except for Northridge, there were only a few or no strong-motion instruments close to the fault. Therefore it is difficult to infer the spatial variation of ground motion from such events. This lack of pertinent data is one of the prime motivations for dynamic simulation studies.

The existing data from dip-slip earthquakes, however, appear to display unique behavior that sets such events apart from more commonly studied vertical strike-slip faults. The 1971 San Fernando [*Nason*, 1973; *Steinbrugge et al.*, 1975] and 1994 Northridge events [*Abrahamson and Somerville*, 1996] produced systematically higher ground motion on the hanging wall. In particular, *Allen et al.* [1998] have shown evidence for vertical accelerations exceeding 1 g at the toe of the hanging wall of the 1971 San Fernando event. There is also evidence that thrust faults have higher dynamic stress drops and produce larger ground motion than normal faults [*McGarr*, 1984; *Cocco and Rovelli*, 1989; *Abrahamson and Somerville*, 1996]. This effect has also been seen in the foam rubber models of *Brune* [1996]. Additionally, the recent Chi-Chi (Taiwan) earthquake has produced an unprecedentedly large data set that displays a strong hanging wall/footwall asymmetry [*Shin et al.*, 2000; *Rau et al.*, 1999; J. K. Chung et al., Ground displacement around the fault of the September 20, 1999, Chi-Chi earthquake, submitted to *Geophysical Research Letters*, 2000, hereinafter referred to as Chung et al., submitted manuscript, 2000].

One key difference between a typical dip-slip fault and a typical strike-slip fault is that dip-slip faults tend to have nonvertical dips, leading to a break in symmetry with respect to the free surface. Because of this geometrical asymmetry the stress field generated by the earthquake must modify itself to match the stress boundary condition at Earth's surface. Therefore the free surface causes a coupling between the shear stress and normal stress on the fault that would not exist either in a whole

[1]Now at Department of Geological Sciences, San Diego State University, San Diego, California.

[2]Now at Istituto Nazionale di Geofisica, Departemento di Scienze Fisiche, Universita di Napoli, Naples, Italy.

Paper number 2000JB900055.
0148-0227/00/2000JB900055$09.00

space or with a vertical fault plane. These variations in normal stress cause variations in the friction on the fault and, consequently, greatly affect the fault motion and near-source seismic radiation.

An alternative way to visualize the situation is to note that dip-slip earthquakes tend to nucleate at depth, with the rupture propagating updip at subsonic speed. Thus seismic waves radiated by the rupture will reflect off the free surface and hit the fault again, modifying the stress field both ahead of and behind the rupture front as it travels toward the surface.

Many researchers have investigated the physics of the earthquake rupture process by numerical simulations [e.g., *Kostrov*, 1966; *Burridge and Halliday*, 1971; *Madariaga*, 1976; *Andrews*, 1976a, b; *Archuleta and Frazier*, 1978; *Day*, 1982a, b; *Ruina*, 1983; *Harris et al.*, 1991; *Harris and Day*, 1993; *Zeng et al.*, 1996; *Perrin et al.*, 1995; *Madariaga and Cochard*, 1996; *Beeler and Tullis*, 1996; *Andrews and Ben-Zion*, 1997; *Ben-Zion and Rice*, 1997; *Nielsen*, 1998; *Shi et al.*, 1998]. Most of these studies have been limited by simplifying approximations required to make the problems manageable, such as placing the fault in an unbounded homogeneous whole space or vertically with respect to a free surface. However, in both these cases the symmetry in the problem eliminates any time variation in the normal stress [*Burridge*, 1973]. Thus, once the waves have left the fault, they are effectively decoupled from the frictional process of the fault rupture. In contrast, a nonvertical fault plane leads to the possibility of seismic waves being reflected from the surface onto the fault plane. Of particular interest is the consequence for the normal stress. This stress would be constant in a whole space or with a vertical strike-slip fault, but it can be time-dependent for a dip-slip fault. Of the few dynamic simulations of dip-slip faulting prior to this work [e.g., *Mikumo and Miyatake*, 1993; *Nielsen*, 1998; *Oglesby et al.*, 1998], only *Nielsen* [1998], *Oglesby et al.* [1998], and *Shi et al.* [1998] have taken the time dependence of normal stress into account in the friction law. Time-dependent normal stress can also arise due to the presence of different materials on the two sides of the fault [*Andrews and Ben-Zion*, 1997; *Ben-Zion and Andrews*, 1998; *Harris and Day*, 1997], to the presence of two or more fault segments [*Harris et al.*, 1991; *Harris and Day*, 1993; *Kase and Kuge*, 1998; *Magistrale and Day*, 1999], and to a nonplanar fault [*Bouchon and Streiff*, 1997; *Kame and Yamashita*, 1999; *Oglesby*, 1999]. Time-dependent normal stress alters both the yield strength of the fault and the sliding frictional stress. Thus it can greatly affect both rupture propagation and slip on the fault. These effects also manifest themselves in differences in ground motion between thrust and normal faults. *Oglesby et al.* [1998] have studied the effects of dipping fault geometry on the dynamics of earthquake rupture, slip, and ground motion. The current study greatly expands on these results, includes the case of buried faults, and directly investigates the effect of normal stress changes on fault rupture.

2. Analytical Approach

To interpret the results of the present dynamic simulations, it is useful to construct an analytical solution for the stresses in the vicinity of the free surface owing to earthquake rupture farther downdip on a dip-slip fault. We assume the simple case of a two-dimensional (plane strain) fault in a homogeneous medium. First, assume that the fault is embedded in a whole space. Let $(\sigma_x, \sigma_y, \sigma_{xy})$ be the components of the incremental stress (relative to an arbitrary equilibrium stress field) due to

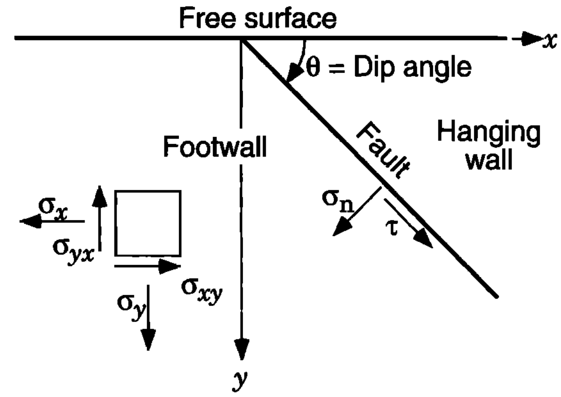

Figure 1. Schematic diagram of the fault geometry, coordinate system, and stress field of a nonvertical dip-slip fault.

the fault rupture, and let $(\sigma_m, \sigma_n, \tau)$ be their projection onto the plane of the fault (Figure 1). For a fault dipping at an angle θ with respect to our x-y coordinate system the relations between the stresses in the two coordinate systems are

$$\begin{aligned}\tau &= \tfrac{1}{2}(\sigma_y - \sigma_x)\sin 2\theta + \sigma_{xy}\cos 2\theta \\ \sigma_n &= \sigma_x \sin^2\theta + \sigma_y\cos^2\theta - 2\sigma_{xy}\sin\theta\cos\theta\end{aligned} \tag{1}$$

$$\begin{aligned}\sigma_x &= \sigma_n\sin^2\theta + \sigma_m\cos^2\theta - 2\tau\sin\theta\cos\theta \\ \sigma_y &= \sigma_n\cos^2\theta + \sigma_m\sin^2\theta + 2\tau\sin\theta\cos\theta \\ \sigma_{xy} &= \tfrac{1}{2}(\sigma_m - \sigma_n)\sin 2\theta + \tau\cos 2\theta.\end{aligned} \tag{2}$$

For an infinite homogenous whole space, symmetry requires $\sigma_m = \sigma_n = 0$, so the projections become

$$\begin{aligned}\tau &= \tfrac{1}{2}(\sigma_y - \sigma_x)\sin 2\theta + \sigma_{xy}\cos 2\theta \\ \sigma_n &= 0\end{aligned} \tag{1'}$$

$$\begin{aligned}\sigma_x &= -2\tau\sin\theta\cos\theta \\ \sigma_y &= +2\tau\sin\theta\cos\theta \\ \sigma_{xy} &= \tau\cos 2\theta.\end{aligned} \tag{2'}$$

Now, if we consider the same fault in a half-space at an angle θ with respect to the free surface, in the vicinity of the free surface (i.e., at depths small with respect to one wavelength), the free surface stress boundary condition at the intersection of the fault and the free surface requires

$$\begin{aligned}\sigma_y^f &= 0 \\ \sigma_{xy}^f &= 0 \\ \sigma_x^f &= 2\sigma_x,\end{aligned} \tag{3}$$

where the superscript f distinguishes the values at the free surface from the values in a whole space. The doubling of the horizontal normal stress at the free surface is not true for a general location on the free surface. However, it can be shown via the static method of *Crouch* [1976] to be true for a point on the surface in the plane of a shear dislocation (S. B. Nielsen and D. D. Oglesby, manuscript in preparation, 2000), regardless of the angle between fault and surface.

By substitution of (3) into (1′) and (2′) we may write the fault stress values in the vicinity of the free surface as a function of the horizontal stress in the whole space:

$$\tau^f = -\sigma_x \sin 2\theta \qquad \sigma_n^f = 2\sigma_x \sin^2 \theta. \tag{4}$$

We can now determine the change in shear and normal stress on the fault due to the presence of the free surface. By taking the difference between (4) and (1′) and performing some algebra, we find for the fault shear stress

$$\tau^f - \tau = -\tfrac{1}{2}(\sigma_x + \sigma_y) \sin 2\theta - \sigma_{xy} \cos 2\theta. \tag{5}$$

Substituting (2′) into (5), we arrive at

$$\tau^f - \tau = -\tau \cos^2 2\theta. \tag{6}$$

Likewise, the same procedure for the normal stress produces

$$\sigma_n^f - \sigma_n = -4\tau \sin^3 \theta \cos \theta. \tag{7}$$

Now we need to determine how these stress changes due to the presence of the free surface affect rupture on the fault. The most simple description of frictional resistance stating the proportionality of strength to normal stress, for both sliding and stationary surfaces with no cohesion, is Amonton's law:

$$|\tau| \geq -\mu\sigma_n, \tag{8}$$

where μ is the static coefficient of friction. If we write $C = |\tau| + \mu\sigma_n$, then the static strength expression can be restated as the fracture criterion $C \geq 0$.

We can now compute the difference in fracture criterion between the whole space and half-space cases, taking into account the modified shear and normal stresses on the fault. We let C represent the fracture criterion for the fault in the whole space and C^f represent the corresponding fracture criterion for the same fault in a half-space close to the surface. Using (6) and (7), we obtain, in the case of a normal fault ($\tau < 0$),

$$C^f - C = -|\tau| \cos^2 2\theta + 4\mu|\tau| \sin^3 \theta \cos \theta. \tag{9}$$

In the case of a thrust fault ($\tau > 0$) we find

$$C^f - C = -|\tau| \cos^2 2\theta - 4\mu|\tau| \sin^3 \theta \cos \theta. \tag{10}$$

Solutions analogous to these were derived by *Nielsen* [1998] for the case of a 45° dipping fault. In the above relations, $C^f - C > 0$ corresponds to the fault being brought closer to failure than it would have been without the free surface, and $C^f - C < 0$ corresponds to the fault being taken farther from failure than it would have been without the free surface. As shown in Figure 2, between dip angles of ~30° and 75°, the normal fault near the surface is brought closer to failure in the presence of a free surface than it would have been in a whole space. Conversely, the thrust fault near the surface is actually taken farther from failure than it would have been in a whole space. Still, for dip angles less than ~55°, the relative fault weakening is greater than -1 and thus corresponds to the fault being brought closer to failure in an absolute sense due to the rupture downdip.

The difference in relative fault weakening between thrust/reverse and normal faults is due to the change in normal stress σ_n across the fault. In the normal faulting case the normal stress magnitude decreases ahead (updip) of the rupture, reducing the yield stress. The converse is true for the thrust fault.

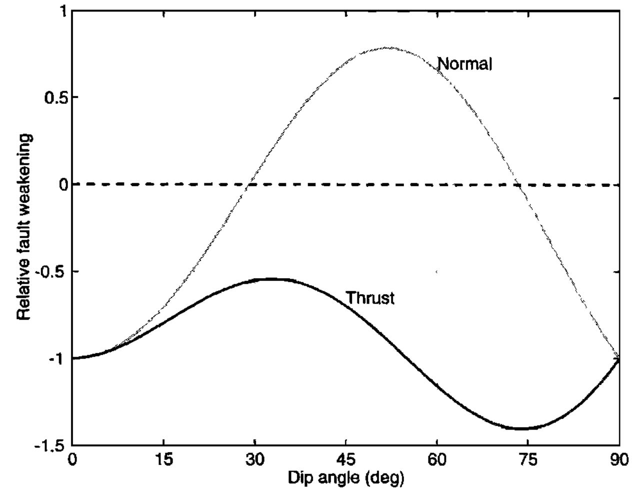

Figure 2. The relative fault weakening $(C^f - C)/\tau$ ahead of the rupture front for a point at the intersection of the free surface and the fault. $(C^f - C)/\tau > 0$ corresponds to aiding rupture compared to the case of a fault in a whole space, and weakening of $(C^f - C)/\tau < 0$ corresponds to hindering rupture compared to the case of a fault in a whole space. However, weakening of $(C^f - C)/\tau > -1$ still corresponds to bringing the fault closer to rupture in an absolute sense.

In the case of the normal fault, the decreased yield stress ahead of the rupture front can drop to the level of the S wave shear stress, causing the fault to have an early secondary nucleation near the free surface, as observed by *Nielsen* [1998] for the case of a 45° dipping fault.

The preceding development has been for points on the fault near the surface that are ahead of the rupture front but have not yet started to slip. Behind the rupture front, in the slipping region of the fault, the stress buildup is replaced by a stress drop: the change in the shear stress for the normal and thrust cases is of the opposite sign. Thus the effects on the normal stress in the slipping region are the opposite of the effects ahead of the rupture: Behind the normal faulting rupture front, the normal stress tends to increase, increasing the sliding friction and decreasing the slip velocity. Conversely, the thrust fault experiences reduced normal stress, decreased sliding friction, and amplified slip velocity.

The above analytical development is limited by the fact that it does not consider dynamic effects such as waves. However, in reality, the stress changes described above are transmitted by seismic waves in the near-surface region and are valid only for regions close to the free surface. Our simple development does not take into account the additional effects of waves reflected off the fault nor does it predict the effect of the free surface on more deeply buried points on the fault. Its purpose is to provide a simple physical argument for understanding the results of the full dynamic simulations to follow. However, as will be seen in the simulation results, through wave phenomena the free surface manifests itself at points even far downdip on the fault.

3. Numerical Simulations

Using a two-dimensional finite element method [*Whirley et al.*, 1992], we simulated the dynamic rupture of dip-slip faults with dip angles of 30°, 45°, and 60°. A key feature of the

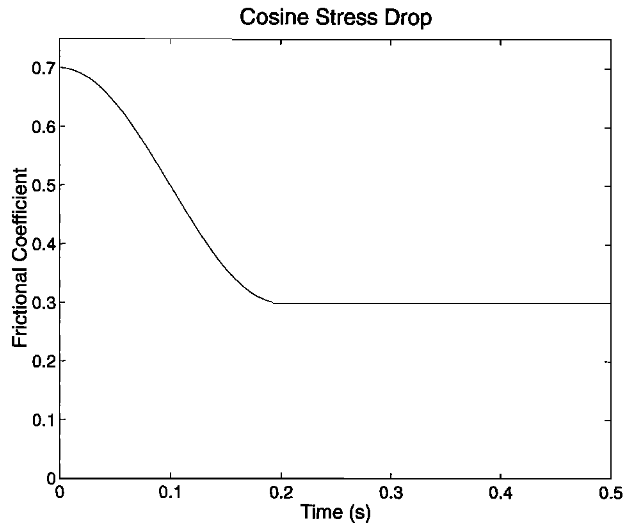

Figure 3. The law used for the reduction of the frictional coefficient μ from its static to its dynamic value. The form is that of a cosine function with a weakening time of 0.2 s.

simulations is that the friction on the fault follows Amonton's law $\tau = \mu\sigma_n$, where τ is the (frictional) shear stress on the fault, μ is the coefficient of friction (either static or sliding), and σ_n is the normal stress. Thus, as the normal stress dynamically changes due to the reflected waves from the surface, the frictional stress also changes, leading to consequences for both the rupture and slip processes. This interaction is a direct result of correctly accounting for the dynamic variations of normal stress on the fault. Additionally, our simulations include a drop from the static frictional level to the dynamic frictional level. When a node on the fault reaches its yield (static frictional level), the node is allowed to slip. After this time, the frictional coefficient drops as a cosine function of time to the sliding frictional level (Figure 3). Such a time-weakening friction law is similar to a slip-weakening friction law [*Ida*, 1972; *Andrews*, 1976a, b] with an effective slip-weakening distance of 1–20 cm, depending on the slip rate. Experiments with a more conventional slip-weakening friction law show that the current results are quite insensitive to whether slip or time is used as the independent variable in the friction. In all cases, fault rupture is nucleated by bringing a small (<1 km) region of the fault above the yield stress. However, experiments with different nucleation methods show that the evolution of rupture and slip is insensitive to the method of nucleation. The fault is healed when the slip velocity turns negative, preventing the fault from rupturing again. Typical numerical parameters in the simulations are summarized in Tables 1 and 2. Experiments with different element sizes indicate that our numerical method is not strongly grid-dependent, with the exception that smaller grids have the ability to propagate higher-frequency signals, and thus can have slightly (~5%) higher peak velocities. However, comparisons between hanging wall and footwall motion and between thrust/reverse and normal fault motion are insensitive to this minor effect.

For all three dip angles the only difference in the initial conditions between the thrust and normal faulting simulations was the sign of the shear stress on the fault. All stress magnitudes and geometrical attributes are identical between the thrust and normal faults. However, as is shown in snapshots of particle velocity for the 45° dipping faults (Plate 1), the resulting fault motions are quite different. Slip is nucleated at $t = 0$ s. For early times ($t = 1.3$ s; $t = 4.9$ s), there is no difference in particle velocity between the normal and thrust faults. This similarity is due to the fact that reflected waves from the surface have not yet greatly affected the normal stress (and thus the frictional stress) on the fault. However, at $t = 7.4$ s the free surface has begun to manifest itself. Owing to the decreased normal stress (and thus decreased yield stress) near the free surface, the rupture front in the normal faulting case has leaped ahead to form a secondary rupture front near the free surface. This secondary rupture front propagates back down the fault to meet the primary rupture front. The thrust fault displays no such effect. At $t = 12.8$ s, both faults have ruptured through to the free surface. In the case of the thrust fault, there is a strong breakout phase [*Burridge and Halliday*, 1971] propagating down the fault from the free surface, implying an amplified dynamic stress drop at the free surface. Owing to both the breakup of the rupture front and the increase in friction after rupture, the normal fault displays no such large phase.

The particle motion described above can be explained by observing the development of the stress field in the vicinity of the 45° dipping normal and thrust faults (Figure 4). In both cases, slip nucleates in the same place, with the only difference being the sign of the shear stress (the absolute value is taken in Figure 4 for ease of comparison). By $t = 2.5$ s a typical shear crack stress pattern [*Ida*, 1972; *Andrews*, 1976a, b] appears on both faults, with a small S wave peak ahead of the crack tip. By $t = 6.6$ s in the case of the normal fault the free surface has started to manifest itself by reducing the normal stress (and hence the yield stress) ahead of the crack tip. Likewise, in keeping with the analytical development the normal stress (and hence the dynamic frictional shear stress) is elevated behind the crack tip in the slipping region. At $t = 6.9$ s the normal stress has decreased even more ahead of the crack tip, so that the yield stress is low enough to trigger rupture at the S wave pulse. Thus the fault has a secondary nucleation, as seen in the velocity snapshots (Plate 1). The secondary rupture front prop-

Table 1. Fault/Material Parameters

Parameter	Value
Fault width (downdip)	28.28 km
Fault dip	30°, 45°, 60°
Shear prestress	2.8 MPa
Normal prestress	6.0 MPa
Static frictional coefficient	0.7
Sliding frictional coefficient	0.3
Density	3000 kg/m^3
Shear modulus	30000 MPa
Poisson's ratio	0.25
V_p	5.48 km/s
V_s	3.16 km/s

Table 2. Computational Parameters

Parameter	Value
Element width on fault	141.4 m
Time increment	1.5×10^{-3} s
Maximum frequency	~2 Hz
Critical slip time	0.2 s
Total time	20 s
Number of elements	~96,000
Run time (UltraSparc 30)	~3–4 hours

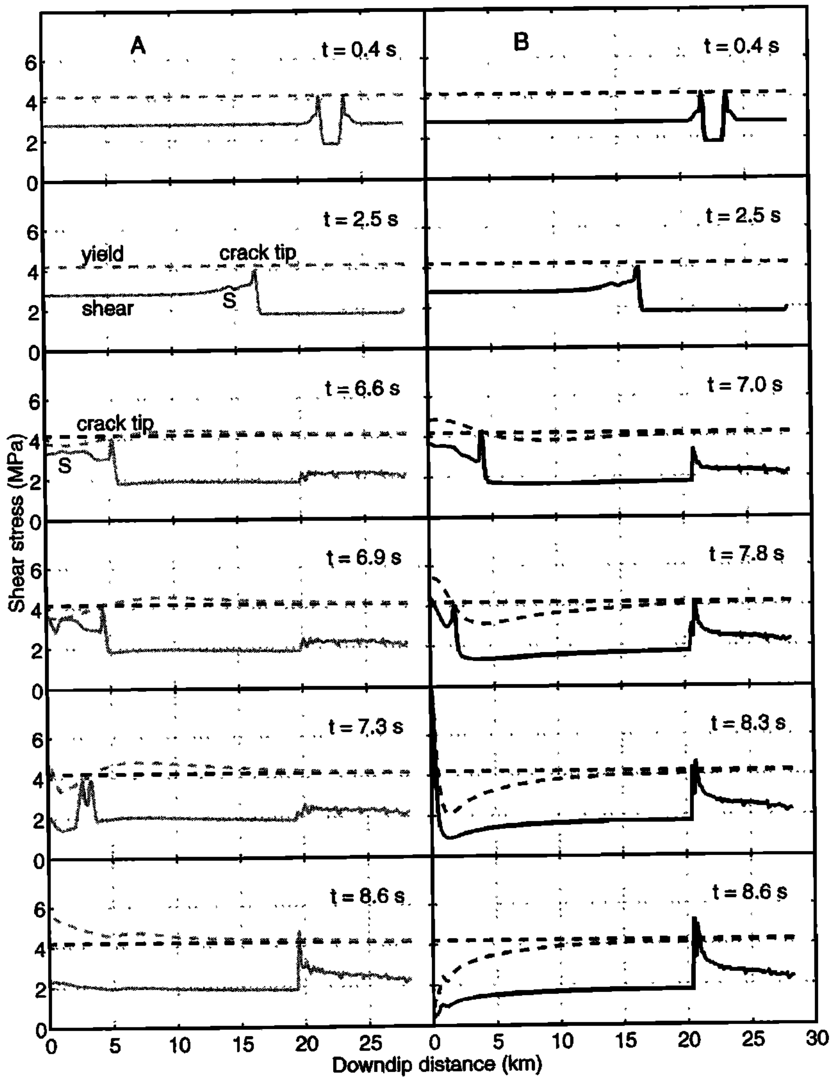

Figure 4. Snapshots of stresses along 45° dipping (a) normal and (b) thrust faults during earthquake rupture. Zero on the horizontal axis corresponds to the free surface, and 28.3 km on the horizontal axis corresponds to the downdip edge of the fault. The solid curves denote shear stress, and the dashed curves denote yield stress. The dashed line denotes the initial yield stress before dynamic stress modification.

agates bilaterally toward the surface and back toward the primary rupture front. By $t = 8.6$ s the entire fault has ruptured, and the normal (and thus also shear) stress near the free surface is still slightly elevated, inhibiting slip. At later times the shear stress in the downdip region of the fault exceeds the yield stress. This artifact is due to the requirement that the fault not slip again after it has healed, but experiments show that the manner of healing does not affect the main results of the simulation: reslipping changes the final state of stress on the fault and makes minor adjustments to the slip but has no effect on the peak velocities.

As the rupture approaches the free surface, the thrust fault behaves quite differently from the normal fault. At $t = 7.0$ s the thrust fault begins to feel the effects of the free surface, as the normal stress and hence the yield stress increase ahead of the crack tip. Similarly, the normal stress and the sliding frictional stress are decreased behind the rupture front, amplifying slip. This effect grows stronger until the crack tip hits the free surface at $t = 8.3$ s. Then, in a very short time the shear stress drops from the greatly increased yield stress to a greatly decreased sliding frictional level. The reduced normal and shear stress further amplifies slip, in agreement with the quasi-static analysis of *Rudniki and Wu* [1995]. The resultant huge dynamic stress drop leads to the strong breakout phase seen in the previous particle velocity snapshots (Plate 1).

It is important to note that for most of the rupture propagation, even though the normal stress is greatly modified, the rupture velocity is not affected for either the normal or thrust fault. The reason for the constant rupture velocity is that for the normal (thrust) fault the crack tip serves as the dividing point between the decreased (increased) normal stress ahead of the crack tip and the increased (decreased) normal stress behind the crack tip. Thus, for most of its propagation the crack tip will experience the same, unmodified yield stress it would have felt without the free surface. The crack tip experiences a modified yield stress in the normal case only when the rupture jumps ahead and in the thrust case only when the rupture front is right at the free surface.

The quantitative effect of the free surface interaction on the fault motion can be seen in the peak particle displacements

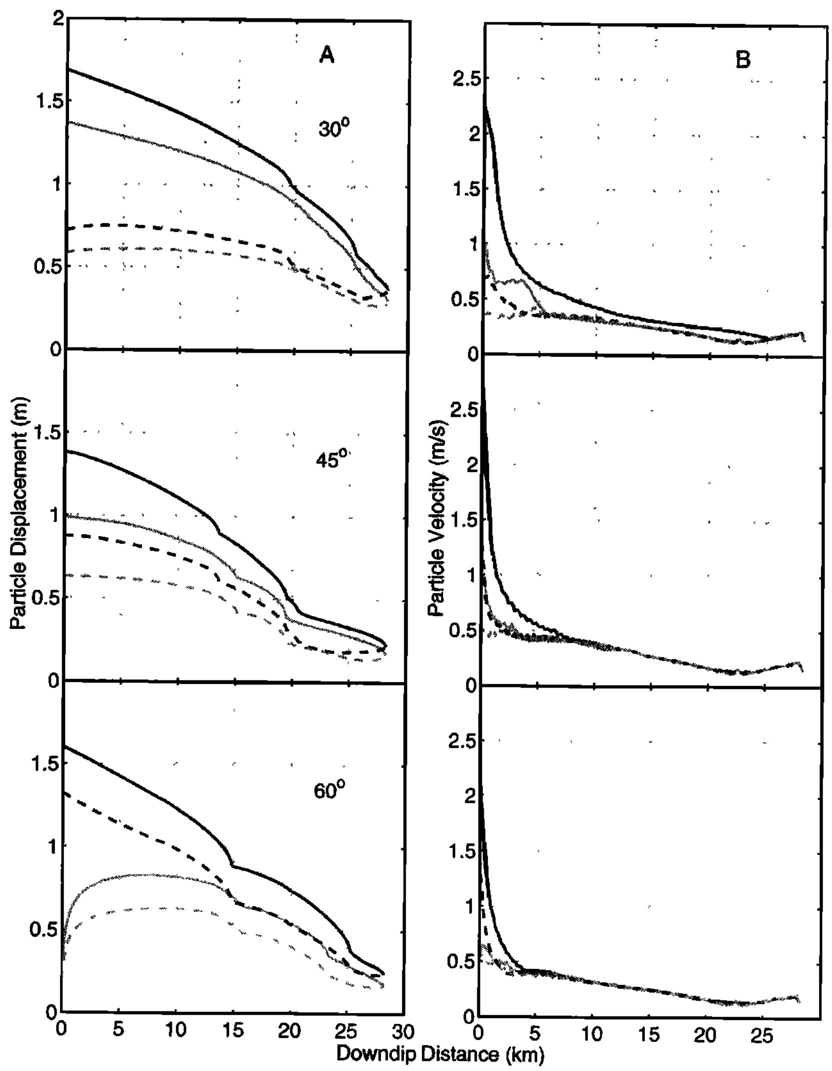

Figure 5. Peak particle (a) displacements and (b) velocities along faults with dips of 30°, 45°, and 60°. Zero on the horizontal axis corresponds to the free surface, and 28.3 km on the horizontal axis corresponds to the downdip edge of the fault. Dark curves denote thrust faults; shaded curves denote normal faults. Solid curves are hanging walls; dashed curves are footwalls.

and velocities on faults with dip angles between 30° and 60° (Figure 5). In all cases, thrust faults have higher displacements and velocities than normal faults. Likewise, the hanging walls have higher displacements and velocities than the footwalls. The higher motion on the hanging wall is another consequence of the asymmetry of the fault with respect to the free surface: Since the hanging wall has less volume and mass near the free surface than the footwall, it will move more under the same stress. Also, since the fault plane is nearly opaque to shear waves as it slips, trapped waves in the hanging wall may contribute to its larger motion. Increased peak velocity and displacement in the hanging wall has also been seen in foam-rubber models [*Brune*, 1996; *Brune and Anooshehpoor*, 1999], dynamic lattice model simulations [*Shi et al.*, 1998], and quasi-static antiplane models [*Davis and Knopoff*, 1991]. As one would expect, as the fault dip angle increases toward 90°, this asymmetry decreases. However, the difference between thrust and normal fault motion actually increases with increasing fault dip. This effect is also seen in our analytical solution (Figure 2), in which the difference in relative fault weakening between the thrust and normal faults increases between 30° and 60° and then rapidly reduces to zero at 90°.

Interestingly, although the free surface effect on peak velocity decreases rapidly as one travels downdip on the fault, the free surface effect on the displacements persists along the entire fault. This effect can be explained in terms of the breakout phase seen previously. For most fault dips the breakout phase is the strongest velocity pulse only near the free surface, so it appears only near the free surface in the peak velocity plots. However, it still contributes to the fault displacement everywhere and thus causes a difference between thrust and normal faulting displacement across the entire fault. The exception is the 30° dipping thrust fault, in which the breakout phase produces an elevated peak velocity over most of the fault plane. Similarly, the difference between hanging wall and footwall motion can only manifest itself after the waves from the fault have "sampled" the free surface and reflected back to the fault. In most cases, these reflected waves produce slip velocities smaller than the initial slip pulse, but they still contribute to the final slip. The radically decreased displacement at the

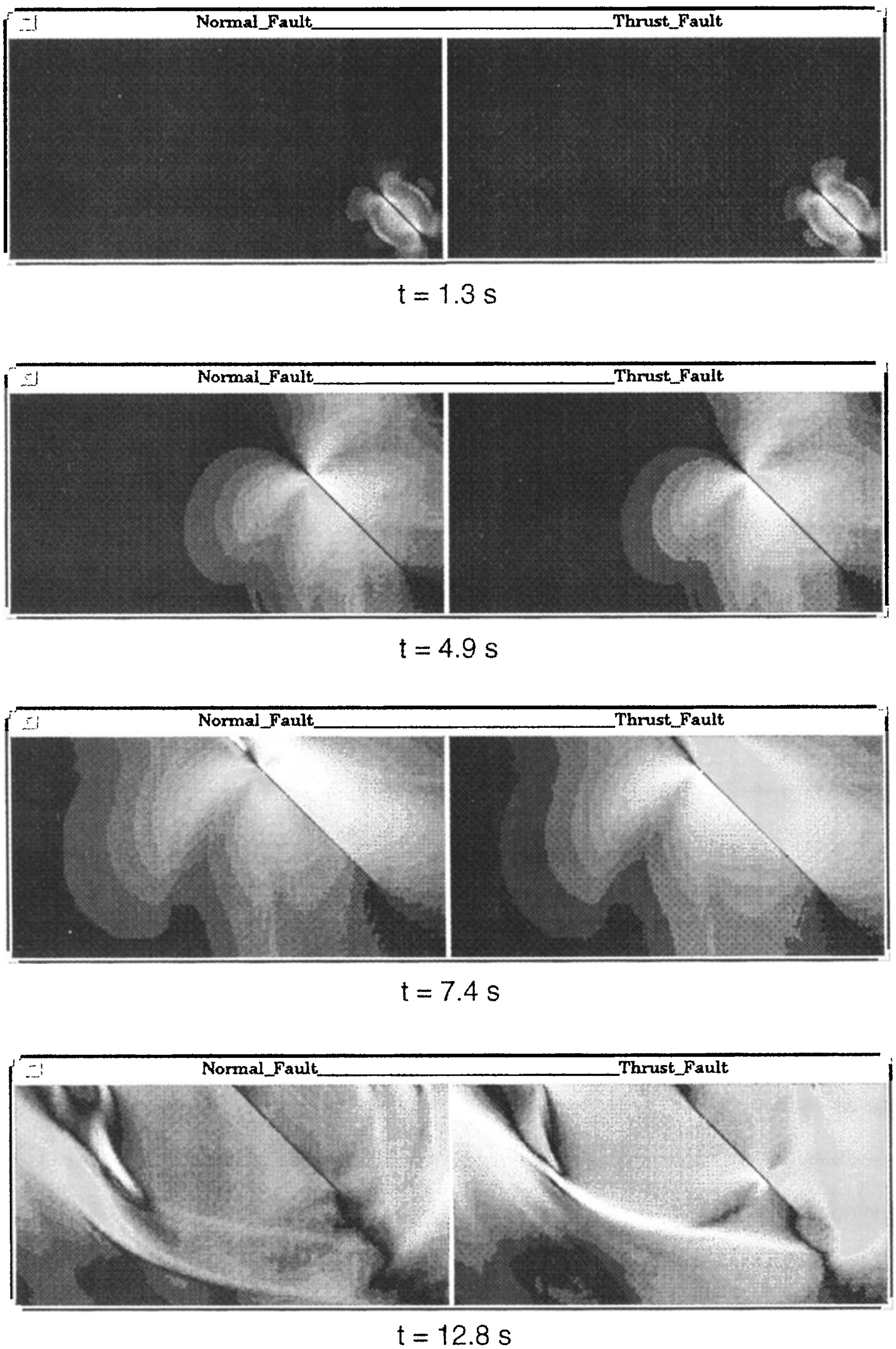

Plate 1. Snapshots of fault-parallel particle velocity for 45° dipping normal and thrust faults during earthquake rupture. The geometry is that of Figure 1. Red corresponds to velocity down and to the right, and blue corresponds to velocity up and to the left. Colors saturate at ±0.1 m/s.

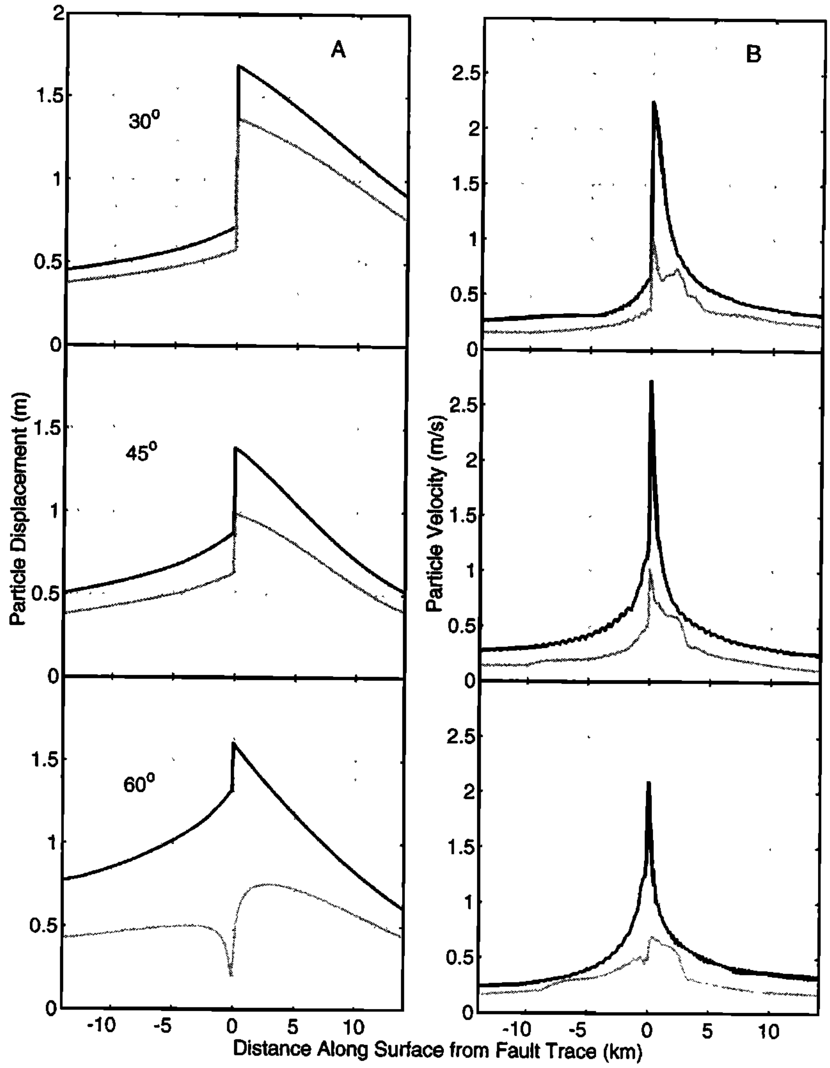

Figure 6. Peak particle (a) displacements and (b) velocities along the free surface above faults with dips of 30°, 45°, and 60°. Zero on the horizontal axis corresponds to the surface trace of the fault; negative distances correspond to the footwall and positive distances correspond to the hanging wall. Dark curves denote thrust faults; shaded curves denote normal faults.

surface of the 60° normal fault is an artifact of the greatly increased normal and frictional stress after rupture. This increased stress causes rapid healing. Since such premature healing has not been observed in nature (albeit with scarce data), it may be an indication that our friction law or healing criterion may not be valid right at the free surface.

The effects of asymmetry with respect to the free surface are also seen in the peak particle displacements and velocities on the free surface in the source vicinity (Figure 6). In all cases, particle motion for the thrust faults is larger than for the normal faults, and there is a large discontinuity in particle displacement and velocity when one crosses over the fault trace from the footwall (negative distances) to the hanging wall (positive distances). Note that while the difference between hanging wall and footwall motion decreases rapidly with distance away from the fault plane, the difference between thrust fault and normal fault motion persists even at large distances. This consistently higher ground motion is largely caused by the increased fault motion near the surface. It is also true that in these simulations the thrust faults have higher slip and consequently higher seismic moments than the normal faults, even though they start with the same initial stress magnitudes. However, scaling the ground motion by the seismic moments reduces but does not eliminate the difference between thrust and normal fault ground motion. Thus, even for the same moment magnitude, thrust faults will produce higher near-source ground motion than normal faults. One interesting feature of the peak surface velocities is the increased peak velocity on the hanging wall of the normal faults, 2–3 km away from the fault trace. This point is the location at which the initial pulses from the secondary rupture front and the primary rupture front arrive simultaneously, greatly increasing the ground velocity.

All the above simulations thus far have been for faults that intersect the Earth's surface. However, many faults (e.g., that of the 1994 Northridge earthquake) are "blind" and do not intersect the free surface. To determine the effect of fault burial on the free surface effects described above, we performed simulations of a 40° dipping fault buried at various depths (Figure 7). When the top of the fault intercepts the surface, we see the same surface ground motion pattern as in

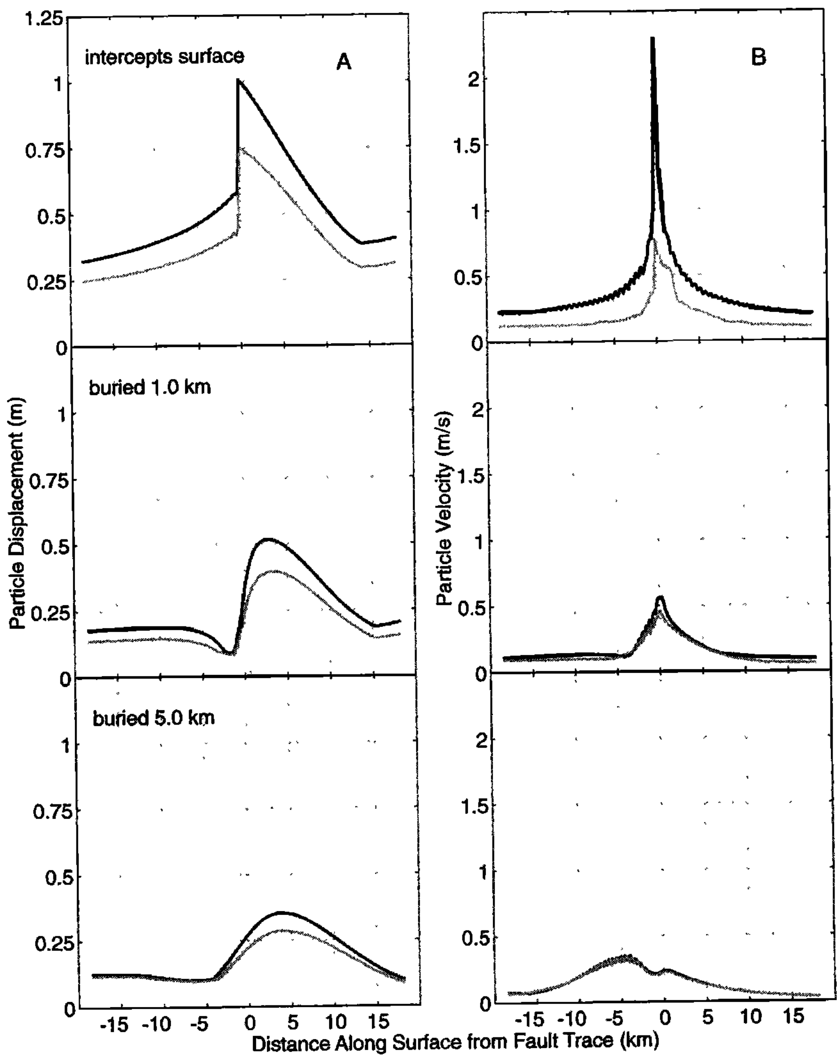

Figure 7. Peak particle (a) displacements and (b) velocities along the free surface above a 40° dipping fault buried at depths of 0, 1.0, and 5.0 km. Zero on the horizontal axis corresponds to the point on the surface directly above the upper edge of the fault; negative distances correspond to the footwall and positive distances correspond to the hanging wall. Dark curves denote thrust faults; shaded curves denote normal faults.

our previous simulations. However, when the top of the fault is buried at a depth of 1.0 km, the differences in peak velocity between the thrust and normal fault, as well as the differences between the hanging wall and footwall motion, almost disappear. This effect has two causes: First, the fault is farther from the free surface, and thus the free surface has less of an effect on rupture. Second, a buried fault is constrained not to move at both its edges, while the updip edge of a fault that intercepts the surface may move freely, greatly amplifying its motion. In fact, simply pinning the updip edge of the fault that intercepts the free surface is enough to reduce the resultant ground motion by half. As the depth of burial increases to 5.0 km (the approximate depth of burial of the Northridge fault), the peak particle velocities show very little effect of the free surface. The free surface effects persist to a greater extent in the peak displacements. Thus we may conclude that while the interaction of the free surface with fault rupture could be very important for faults that intersect the free surface, the importance of this effect decreases rapidly with burial depth.

Another issue in these simulations is the cause of the difference between thrust and normal faulting. Previous studies [e.g., *Mikumo and Miyatake*, 1993] have simulated dip-slip faults, but without taking into account the time variability of normal stress in their friction laws. To determine the effects of this omission (all other attributes being equal), we have simulated the (artificial) case in which the friction depends not on the time-dependent dynamic normal stress, but only on the constant normal prestress. Thus $\tau = \mu\sigma_{n0}$, where σ_{n0} is constant, and the only variation in fault friction is due to the drop in μ from its static to its sliding value. Figure 8 shows that when the effect of time-dependent normal stress is removed from the simulation, the resulting thrust and normal faults produce the same ground motion pattern, which is almost exactly halfway in between the true thrust and normal ground motions. This simulation indicates that the time dependence of normal stress is, in fact, the cause of the difference between thrust/reverse and normal fault motion and that the omission of time-dependent normal stress can lead to inaccurate results.

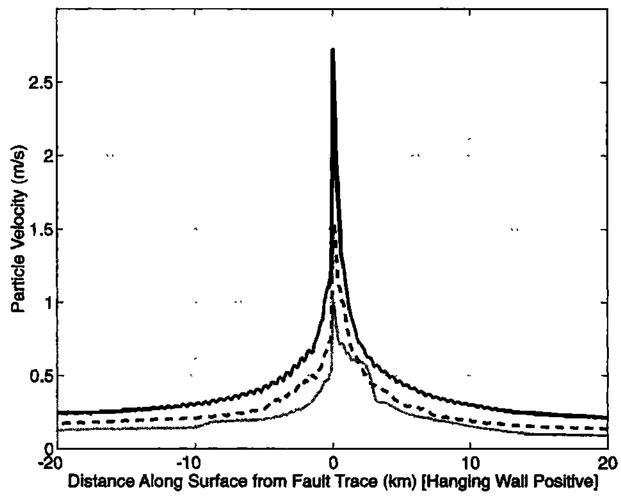

Figure 8. Peak particle velocities along the free surface above a 45° dipping fault. The dark solid curve denotes the peak velocity for a thrust fault, and the shaded solid curve denotes the peak velocity for a normal fault. The dashed curve displays the overlaid peak velocities for both thrust and normal faults in which the time dependence of normal stress has been removed from the frictional stress calculation.

4. Conclusions

The results of our simulations may explain observations of ground motion in the vicinity of dip-slip faults, such as stronger ground motion from thrust faults than from normal faults and stronger ground motion on the hanging wall than on the footwall. The larger motion of the hanging wall will cause increased strain in the hanging wall. This effect could provide an explanation for the cloud of aftershocks often seen in the hanging wall after dip-slip earthquakes. Fortunately, the amplified ground motion from a thrust fault appears to decay rapidly with the depth of burial of the fault, so the ground motion from "blind thrusts" may not be as substantial as the motion from faults that extend all the way to the free surface. Finally, the simulations indicate that in order to predict the ground motion from a dip-slip earthquake the time-dependent normal stress must be included in the friction law. Otherwise, the tendency will be to overestimate the motion of the normal fault and underestimate the motion of the thrust fault.

While this current work was under review, the 1999 Chi-Chi (Taiwan) earthquake produced a large set of near-source data that verifies some of the predictions made in this paper. Early analyses of the strong-motion data [*Shin et al.*, 2000; Chung et al., submitted manuscript, 2000] and Global Positioning System (GPS) data [*Rau et al.*, 1999] indicate that the hanging wall experienced much higher displacement and peak velocity than the footwall, with a strong discontinuity at the fault trace. The ground motion pattern of this earthquake is quite similar to that predicted in the current two-dimensional dynamic models. A more specific investigation of the effects of the dipping fault geometry on this earthquake is in progress (D. D. Oglesby and S. M. Day, manuscript in preparation, 2000). However, a comparison between the current model and the actual Chi-Chi data strongly implies that for thrust earthquakes that rupture through to the free surface, the fault/free surface interaction can have a very large effect on the fault slip and ground motion.

There are some caveats to our results. First, since the models are two-dimensional, more energy is concentrated near the crack tip than would be in the case of a full three-dimensional simulation. It could be argued that this effect could lead to an overestimate of the effect of the free surface on rupture dynamics. However, future work [*Oglesby et al.*, 2000] will show that three-dimensional models produce results very similar to the two-dimensional results in this work. Second, it is possible that in a tensional tectonic regime the normal stress on faults near the free surface may be tensile, thus removing the normal stress factor from the friction law (Y. Zeng, personal communication, 1997). However, simulations in which the stress drop tapered to zero in the upper few hundred meters produced essentially the same results as in the current work. Third, it is also possible that friction in the upper 1 or 2 km may be greatly affected by rock weakness and/or pore pressure, so that the upper portions of faults may not hold much fracture energy. Thus our simulations should be thought of as limiting cases, in which the stress drop extends all the way to the free surface. Finally, we use a rather simple-minded friction law, whereas there is laboratory evidence that more complicated (e.g., rate-weakening, rate-and-state) friction may be operating on faults in nature [e.g., *Dieterich*, 1979]. In spite of these limitations the results of this study are robust and illuminate the possibility that through knowledge of fault geometry, researchers may be able to predict many features of future earthquakes.

Acknowledgments. Computations for this study were carried out primarily on the SGI Origin 2000 at the Materials Research Laboratory, UCSB (NSF grant CDA96-01954). This research was supported by the University of California, Santa Barbara; UCSB/CLC grant 08950868; and LLNL/IGPP grant 98-GS012. Support for S. Nielsen was provided by the MRSEC Program of the National Science Foundation under award DMR96-32716. The authors gratefully acknowledge the extensive programming advice of Edward Zywicz and the support and advice of William Foxall, Lawrence Hutchings, Steve Day, and Kim Olsen. This manuscript benefited greatly from insightful reviews by Nadia Lapusta, Dudley J. Andrews, and Yehuda Ben-Zion. This work is ICS contribution 0286-69EQ.

References

Abrahamson, N., and P. Somerville, Effects of the hanging wall and footwall on ground motions recorded during the Northridge earthquake, *Bull. Seismol. Soc. Am.*, *86*, S93–S99, 1996.

Allen, C. R., J. N. Brune, L. S. Cluff, and A. G. Barrows, Evidence for unusually strong near-field ground motion on the hanging wall of the San Fernando fault during the 1971 earthquake, *Seismol. Res. Lett.*, *69*, 524–531, 1998.

Andrews, D. J., Rupture propagation with finite stress in antiplane strain, *J. Geophys. Res.*, *81*, 3575–3582, 1976a.

Andrews, D. J., Rupture velocity of plane strain shear cracks, *J. Geophys. Res.*, *81*, 5679–5687, 1976b.

Andrews, D. J., and Y. Ben-Zion, Wrinkle-like slip pulse on a fault between different materials, *J. Geophys. Res.*, *102*, 553–571, 1997.

Archuleta, R. J., and G. A. Frazier, Three-dimensional numerical simulations of dynamic faulting in a half-space, *Bull. Seismol. Soc. Am.*, *68*, 541–572, 1978.

Beeler, N. M., and T. E. Tullis, Self-healing slip pulses in dynamic rupture models due to velocity-dependent strength, *Bull. Seismol. Soc. Am.*, *86*, 1130–1148, 1996.

Ben-Zion, Y., and D. J. Andrews, Properties and implications of dynamic rupture along a material interface, *Bull. Seismol. Soc. Am.*, *88*, 1085–1094, 1998.

Ben-Zion, Y., and J. R. Rice, Dynamic simulations of slip on a smooth fault in an elastic solid, *J. Geophys. Res.*, *102*, 17,771–17,784, 1997.

Bouchon, M., and D. Streiff, Propagation of a shear crack on a nonplanar fault: A method of calculation, *Bull. Seismol. Soc. Am.*, *87*, 61–66, 1997.

Brune, J., Particle motions in a physical model of shallow angle thrust faulting, *Proc. Indian Acad. Sci. Earth Planet. Sci.*, *105*, L197–L206, 1996.

Brune, J. N., and A. Anooshehpoor, Dynamic geometrical effects on strong ground motion in a normal fault model, *J. Geophys. Res.*, *104*, 809–815, 1999.

Burridge, R., Admissible speeds for plane-strain self-similar shear cracks with friction but lacking cohesion, *Geophys. J. R. Astron. Soc.*, *35*, 439–455, 1973.

Burridge, R., and G. S. Halliday, Dynamic shear cracks with friction as models for shallow focus earthquakes, *Geophys. J. R. Astron. Soc.*, *25*, 261–283, 1971.

Cocco, M., and A. Rovelli, Evidence for the variation of stress drop between normal and thrust faulting earthquakes in Italy, *J. Geophys. Res.*, *94*, 9399–9416, 1989.

Crouch, S. L., Solution of plane elasticity problems by the displacement discontinuity method, *Int. J. Numer. Methods Eng.*, *10*, 301–343, 1976.

Davis, P. M., and L. Knopoff, The dipping antiplane crack, *Geophys. J. Int.*, *106*, 581–585, 1991.

Day, S. M., Three-dimensional finite difference simulation of fault dynamics: Rectangular faults with fixed rupture velocity, *Bull. Seismol. Soc. Am.*, *72*, 705–727, 1982a.

Day, S. M., Three-dimensional simulation of spontaneous rupture: The effect of nonuniform prestress, *Bull. Seismol. Soc. Am.*, *72*, 1881–1902, 1982b.

Dieterich, J. H., Modeling of rock friction, 1, Experimental results and constitutive equations, *J. Geophys. Res.*, *84*, 2161–2168, 1979.

Harris, R. A., and S. M. Day, Dynamics of fault interaction: Parallel strike-slip faults, *J. Geophys. Res.*, *98*, 4461–4472, 1993.

Harris, R. A., and S. M. Day, Effects of a low-velocity zone on a dynamic rupture, *Bull. Seismol. Soc. Am.*, *87*, 1267–1280, 1997.

Harris, R. A., R. J. Archuleta, and S. M. Day, Fault steps and the dynamic rupture process: 2-D numerical simulations of a spontaneously propagating shear fracture, *Geophys. Res. Lett.*, *18*, 893–896, 1991.

Ida, Y., Cohesive force across the tip of a longitudinal-shear crack and Griffith's specific surface energy, *J. Geophys. Res.*, *77*, 3796–3805, 1972.

Kame, N., and T. Yamashita, A new light on arresting mechanism of dynamic earthquake faulting, *Geophys. Res. Lett.*, *26*, 1997–2000, 1999.

Kase, Y., and K. Kuge, Numerical simulation of spontaneous rupture process on two non-coplanar faults: The effect of geometry on fault interaction, *Geophys. J. Int.*, *135*, 911–922, 1998.

Kostrov, B. V., Unsteady propagation of longitudinal shear cracks, *J. Appl. Math. Mech.*, *30*, 1241–1248, 1966.

Madariaga, R., Dynamics of an expanding circular fault, *Bull. Seismol. Soc. Am.*, *66*, 639–666, 1976.

Madariaga, R., and A. Cochard, Dynamic friction and the origin of the complexity of earthquake sources, *Proc. Natl. Acad. Sci. U. S. A.*, *93*, 3819–3824, 1996.

Magistrale, H., and S. Day, 3D simulations of multi-segment thrust fault rupture, *Geophys. Res. Lett.*, *26*, 2093–2096, 1999.

McGarr, A., Scaling of ground motion parameters, state of stress, and focal depth, *J. Geophys. Res.*, *89*, 6969–6979, 1984.

Mikumo, T., and T. Miyatake, Dynamic rupture processes on a dipping fault, and estimates of stress drop and strength excess from the results of waveform inversion, *Geophys. J. Int.*, *112*, 481–496, 1993.

Mikumo, T., T. Miyatake, and M. A. Santoyo, Dynamic rupture of asperities and stress changes during a sequence of large interplate earthquakes in the Mexican subduction zone, *Bull. Seismol. Soc. Am.*, *88*, 686–702, 1998.

Nason, R., Increased seismic shaking above a thrust fault, in *San Fernando, California, Earthquake of February 9, 1971*, vol. III, edited by L. Murphy, pp. 123–126, U.S. Dep. of Commer., Natl. Oceanic and Atmos. Admin., Silver Spring, Md., 1973.

Nielsen, S. B., Free surface effects on the propagation of dynamic rupture, *Geophys. Res. Lett.*, *25*, 125–128, 1998.

Oglesby, D. D., Earthquake dynamics on dip-slip faults, Ph.D. thesis, Univ. of Calif., Santa Barbara, 1999.

Oglesby, D. D., R. J. Archuleta, and S. B. Nielsen, Earthquakes on dipping faults: The effects of broken symmetry, *Science*, *280*, 1055–1059, 1998.

Oglesby, D. D., R. J. Archuleta, and S. B. Nielsen, The three-dimensional dynamics of dipping faults, *Bull. Seismol. Soc, Am.*, in press, 2000.

Perrin, G., J. R. Rice, and G. Zheng, Self-healing slip pulse on a frictional surface, *J. Mech. Phys. Solids*, *43*, 1461–1495, 1995.

Rau, R., J. Yu, T. Yu, M. Yang, and C. Tseng, Co-seismic displacements of the 1999 Chi-Chi, Taiwan, earthquake sequence, paper presented at Fall Meeting, *AGU*, San Francisco, Calif., 1999.

Reagor, G., and F. W. Baldwin, Intensity survey of the Borah Peak, Idaho, earthquake of October 28, 1983, *U.S. Geol. Surv. Open File Rep., OF 84-0166 0196-1497*, 1984.

Romney, C. F., Seismic waves from the Dixie Valley–Fairview Peak earthquakes, *Bull. Seismol Soc Am.*, *47*, 301–319, 1957.

Rudnicki, J., and M. Wu, Mechanics of dip-slip faulting in an elastic half-space, *J. Geophys. Res.*, *100*, 22,173–22,186, 1995.

Ruina, A., Slip instability and state variable friction laws, *J. Geophys. Res.*, *88*, 10,359–10,370, 1983.

Shakal, A., et al., CSMIP strong-motion records from the Petrolia, California earthquakes of April 25–26, 1992, *Calif. Strong Motion Instrum. Program Rep. OSMS 92-05*, Calif. Div. of Mines and Geol., Sacramento, 1992.

Shakal, A., et al., CSMIP strong-motion records from the Northridge, California earthquake of 17 January 1994, *Calif. Strong Motion Instrum. Program Rep. OSMS 94-07*, Calif. Div. of Mines and Geol., Sacramento, 1994.

Shi, B., A. Anooshehpoor, J. N. Brune, and Y. Zeng, Dynamics of thrust faulting: 2D lattice model, *Bull. Seismol. Soc. Am.*, *88*, 1484–1494, 1998.

Shin, T. C., K. W. Kuo, W. H. Lee, T. L. Teng, and Y. B. Tsai, A preliminary report on the 1999 Chi-Chi (Taiwan) earthquake, *Seismol. Res. Lett.*, *71*, 24–30, 2000.

Steinbrugge, K., E. E. Scader, and D. F. Moran, Building damage in San Fernando Valley, in *San Fernando, California, Earthquake of 9 February 1971*, edited by G. Oakeshott, *Calif. Div. Mines Geol. Bull. 196*, 323–353, 1975.

Trifunac, M. D., and D. E. Hudson, Analysis of the Pacoima Dam accelerogram—San Fernando, California, earthquake of 1971, *Bull. Seismol. Soc. Am.*, *61*, 1393–1411, 1971.

U.S. Coast and Geodetic Survey, Preliminary report, Hebgen Lake, Montana, earthquake, August 1959, Washington, D. C., 1959.

Whirley, R. G., B. E. Engelmann, and J. O. Hallquist, DYNA2D: A nonlinear, explicit, two-dimensional finite element code for solid mechanics—User manual, *Rep. UCRL-MA-110630*, Univ. of Calif., Lawrence Livermore Natl. Lab., Livermore, Calif., 1992.

Zeng, Y., B. Shi, and J. N. Brune, Dynamic simulation of shallow angle thrust faulting, *Eos Trans. AGU*, *77*(46), Fall Meet. Suppl., F505, 1996.

R. J. Archuleta, Department of Geological Sciences, University of California, Santa Barbara, CA 93106-1100. (ralph@quake.crustal.ucsb.edu)

S. B. Nielsen, Istituto Nazionale di Geofisica, Departemento di Scienze Fisiche, Universita di Napoli Federico II, Via Cintia 45 (Monte S. Angelo), I-80126 Naples, Italy. (snielsen@na.infn.it)

D. D. Oglesby, Department of Geological Sciences, San Diego State University, 5500 Campanile Drive, San Diego, CA 92182-1020. (doglesby@moho.sdsu.edu)

(Received August 5, 1999; revised January 27, 2000; accepted February 22, 2000.)